Preparation of Multiwall Carbon Nanotubes/ Poly(*p*-phenylene benzobisoxazole) Nanocomposites and Analysis of Their Physical Properties

X. Li, Y. D. Huang, L. Liu, H. L. Cao

Department of Applied Chemistry, Faculty of Science, Harbin Institute of Technology, Harbin 150001, People's Republic of China

Received 31 March 2006; accepted 4 April 2006
DOI 10.1002/app.24649
Published online in Wiley InterScience (www.interscience.wiley.com).

ABSTRACT: Raw multiwall carbon nanotubes (MWNTs) were first treated with strongly oxidated acid to form MWNTs–COOH and driven to a high dispersion quality in the dispersing medium via ultrasonic method. Then the MWNTs/poly (*p*-phenylene benzobisoxazole)(MWNTs–COOH/PBO) nanocomposites were prepared by an *in situ* polymerization technique. In this process, the morphological structure of MWNTs and MWNTs–COOH were investigated by XPS, FTIR, and TEM. The experimental results showed that the carboxyl group was introduced into the surface of nanotubes and the length of nanotubes was shortened. The images of SEM and AFM illustrated that the MWNTs–COOH was homogeneously dispersed in PBO matrix, and the DTA analysis indicated that the molecular weight of MWNTs–COOH/PBO was almost equal to that of PBO. Furthermore, the thermogravimetry results proved that the thermal property of MWNTs–COOH/PBO was more stable than that of PBO. Also, the knot strength and the tensile strength of MWNTs–COOH/PBO were 30% higher than that of PBO. In addition, the reaction route of the MWNTs–COOH and PBO oligomer was given according to the ATR–FTIR spectra of PBO polymer and MWNTs–COOH/PBO. J Appl Polym Sci 102: 2500–2508, 2006

Key words: nanocomposites; synthesis; structure; oligomers

INTRODUCTION

Poly-*p*-phenylene benzobisoxazole (PBO) (Fig. 1) is prepared by polycondensation of 4,6-diamionophenol dihydrochloride(DADHB 2HCl) and terephthalic acid in PPA (poly (phosphoric acid)).[1] So Ying-Hung et al.[2] proposed the mechanism for PBO polymerization, that is, both chain ends were capped with DADHB, and the structure of the PBO oligomer is shown in Figure 2(b).

The PBO polymer has many excellent properties, such as thermal and oxidative stability, good hydrolytic and solvent resistance,[3–5] etc. And PBO fibers have remarkable Young's modulus and tensile strength.[6] But there exists a problem of relatively low axial compressive strength compared with carbon and glass fibers,[7] which limits the use of PBO in composites. This relatively poor axial compressive strength of PBO is mainly ascribed to the weak lateral interactions between the molecules. Until now, a lot of research efforts[8–10] have been expended in attempting to improve the fiber compressive strengths. Most of the methods have been aimed at modifying the molecular structures to improve the interactions between the chains by introducing hydrogen bonding and disrupting chain packing. But there is no significant improvement observed in compressive strength at present.[11] Reactive resin-infiltrated PBO fibers are exposed to irradiation, and their compressive strength is slightly enhanced; there is also an increase in their tensile strength and elongation to break.[12] Inorganic components are also introduced into PBO to improve the compressive behavior. PBO/SWNT[13] has been reported that the presence of 10 wt % SWNT led to a 50% increase in tensile strength. But the cost of single-walled nanotubes (SWNTs) is much higher than that of MWNTs.

Since the discovery of carbon nanotubes (CNTs),[14] more and more researchers are interested in the field of CNT/polymer nanocomposites.[15,16] The CNTs are expected to serve as mechanical reinforcements for lightweight composites systems with the further promise of multifunctionality. In fact, no matter how the nanotubes powders are produced, CNTs always contain some impurities such as amorphous carbons, fullerenes, and nanocrystalline graphite, as well as transition metals that are introduced as a catalyst.

Correspondence to: Y. D. Huang (huangyd@hit.edu.cn).
Contract grant sponsor: National Natural Science Foundation of China; contract grant number: 50333030.
Contract grant sponsor: The Outstanding Youth Foundation of Heilongjiang Province of China; contract grant number: JC04-12.

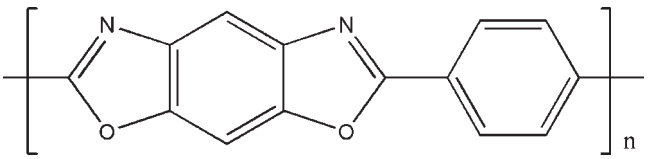

Figure 1 Structure of PBO.

Moreover, smooth surface of CNTs can not contain functional groups, thereby lack in interfacial bonding. CNTs tend to remain as entangled agglomerates, and homogeneous dispersion of CNTs in matrix is not easily obtained. So CNTs/polymer composites have bad mechanical properties. CNTs are typically pulled out from the matrix rather than fractured, and play a limited reinforcement role.[17–19] The dispersion property becomes more and more important when CNTs are blended into the polymer. The shortcoming limits the best performance of CNTs applications to new functional devices. Therefore, a fine and homogeneous dispersion of CNTs in polymer matrix is considered one of the key factors.[20] Although a number of studies have focused on the dispersion of CNTs, complete dispersion of CNTs in a polymer matrix has rarely been achieved. Most dispersion studies have been directed toward chemical modification of the CNT surface.[21–23] This method of chemical oxidation not only dissolves any residual metal catalyst but also removes the CNTs end cap where carboxylic acid (—COOH) is introduced [Fig. 2(a)]. From the viewpoint of molecular design, PBO oligomer could react with nanotubes containing —COOH.

In this study, raw MWNTs were first treated with acid to form MWNTs–COOH, and then dispersed in the medium by ultrasonic. The MWNTs–COOH/PBO is synthesized in PPA using typical PBO polymerization conditions. The dispersion of nanotubes in the PBO matrix was evaluated according to the images of SEM and AFM. The mechanical and thermal properties of MWNTs–COOH/PBO were compared with that of PBO.

EXPERIMENTAL

Raw materials

The MWNTs prepared by thermal vapor deposition method were obtained from Shenzhen Nanotech Port Co., China. All other chemicals were purchased and used directly without any treatment.

Characterization

Fourier Transform Infrared (FTIR) spectra were taken on a Nicolet FTIR analyzer (Nexus 670). The raw and treated MWNTs were tested by KBr disk method. PBO and MWNTs–PBO fibers were tested by attenuated total reflection–Fourier Transform Infrared (ATR–FTIR).

X-ray photoelectron spectroscopy (XPS) was adopted to measure the surface compositions of the nanotubes. The measurements were performed using a VG Scientific Esca-lab MK II spectrometer equipped with a monochromatic Mg Kα X-ray source (1253.6 eV). The instrument was operated with an analyzer chamber pressure of 2.6×10^{-7} Pa, and with the axis of the energy analyzer at 90°C relative to the nominal plane of the sample surface and operated in fixed transmission mode.

The Raman spectrum was recorded with a T64000 Raman spectrometer equipped with an Ar^+ gas laser (514.532 nm) (JY Co., France). The Raman band of a silicon wafer at 520 cm^{-1} was used to calibrate the spectrometer. The laser power at the sample was 100 mW. The laser beam was focused on the samples using an optical microscope with a 50× objective lens. The spectral resolution was 0.15 cm^{-1}.

Thermogravimetric analysis (TGA) and differential thermal analysis (DTA) were performed on the NETZSCH simultaneous thermal analyzer (STA-449C, made in Germany). Samples weighting about 10.0 mg were heated from 30°C to 800°C at a heating rate of 10°C min^{-1} in nitrogen or air atmosphere.

The measuring test of knot strength was carried out with universal tensile tester (Model DCS-5000, Shimadzu) at 25°C according to China GB/T14337-93. The head speed was 10 mm/min. All measurements were made several times and the resulting values were averaged. The schematic of these methods was shown in Figure 3.

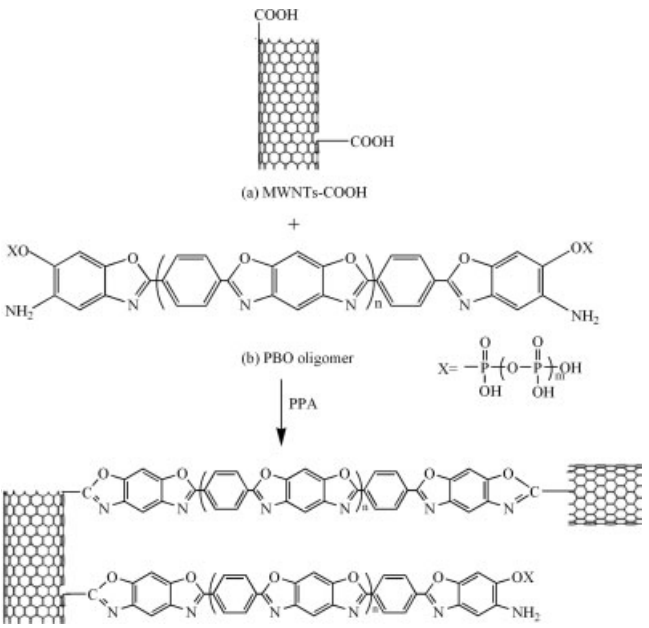

Figure 2 The reaction route of MWNTs–COOH and PBO oligomer.

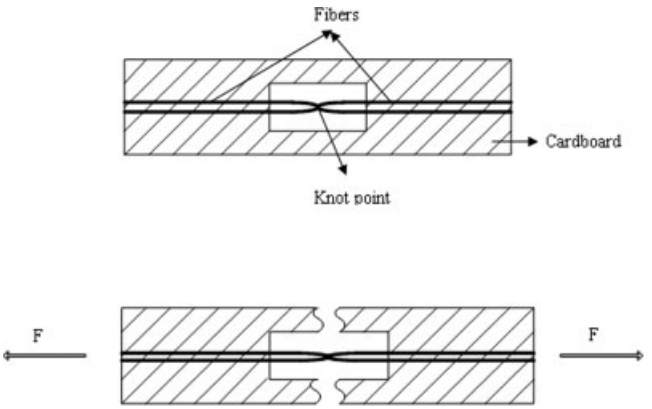

Figure 3 Schematic methods for knot strength of fibers.

A JEOL JEM-1200ZY transmission electron microscope from Japan was used to observe microstructure of the samples at 100 kV. The samples were dispersed in 95% ethanol by ultrasonication for 10 min in a KQ-50 ultrasonic bath, and then they were dropped onto a copper grid.

A HITACHI *S*-4700 scanning electron microscope (Hitachi, Japan) was used to observe microstructure of the samples at an accelerating voltage of 15 kV. The samples were coated with a thin layer of gold before observation.

The morphologies of MWNTs–COOH/PBO nanocomposites and raw MWNTs/PBO surface were examined using a Solver P47 atomic force microscope (NT-MDT Corp., Russia). All images were obtained in the noncontact mode at room temperature. The scanning scope was $4 \times 4\ \mu m^2$.

Purification and acid treatment of MWNTs

The raw MWNTs (Shenzhen Nanotech Port) were treated to attach the carboxylic acid groups to the nanotubes surface. The procedure of acid treatment[24] was the following: firstly, 1.5 g portion of raw MWNTs was added to 200 mL of mixing acid of concentrated sulfuric acid (98%) and nitric acid (68%) (1/3 by volume); secondly, the mixture was treated with a reflux process at 100°C for 3 h; thirdly, the mixture was diluted with distilled water, followed by filtering through PTFE filler (0.2 μm pore size) and washed with an excess of water until no residual acid was present; finally, the samples were dried at 80°C under vacuum.

Preparation of composites and polymer

4,6-diamionophenol dihydrochloride(DADHB 2HCl) was prepared through a three-step reaction from trichlorobenzene[25] and was purified by recrystallization from diluted hydrochloric aqueous solution with $SnCl_2$. Terephthalic acid (TA) was ground fine with ball mill and was dried in a vacuum oven for 5 h at 100°C before it was used.

All glassware and stirring bars were oven-dried before used. 25 mmol DADHB and 25 mmol TA were mixed together with freshly prepared 83 wt % polyphosphric acid (PPA) (25.30 g) in a 100 mL glass flask equipped with a mechanical stir and two gas ports. Removal of HCl from DADHB 2HCl was performed under 100°C for 20 h under nitrogen atmosphere and subsequently at 140°C for 4 h. At this stage, 10.487 g mixture containing H_3PO_4 and MWNTs–COOH (the MWNTs concentration was 5 wt % with respect to the PBO polymer) by ultrasonic for 30 min under room temperature was first added to the reaction flask, and then 21.11 g fresh P_2O_5 was added to the mixtures in the reaction flask in multiple times to make the final P_2O_5 concentration to 83 wt %. The mixture was heated at 160°C for 24 h with constant and strong stirring. Stir opalescence was observed, indicating the appearance of the nematic phase.[26] The mixture was finally heated to 200°C for 6 h with stirring. The composites dope was spun by dry–wet spinning technique. The detailed spinning conditions were listed as follows:

The diameter of spinneret was 40 μm, the length of air gap was 25 cm, the draw ratio was 50, the spinning temperature was 200°C and the water was used as coagulation. The fibers were first washed to remove PPA in distilled water, then dipped into DMSO and extracted by using distilled water, at last dried under vacuum at 100°C. The fibers were tested without high temperature treatment.

Under the same condition, PBO were prepared with DADHB 2HCl and TA in PPA and spun to fibers. Raw MWNTs/PBO composites were prepared, but could not be spun to fibers. The PBO polymer, MWNTs–COOH/PBO nanocomposites, and concentrations

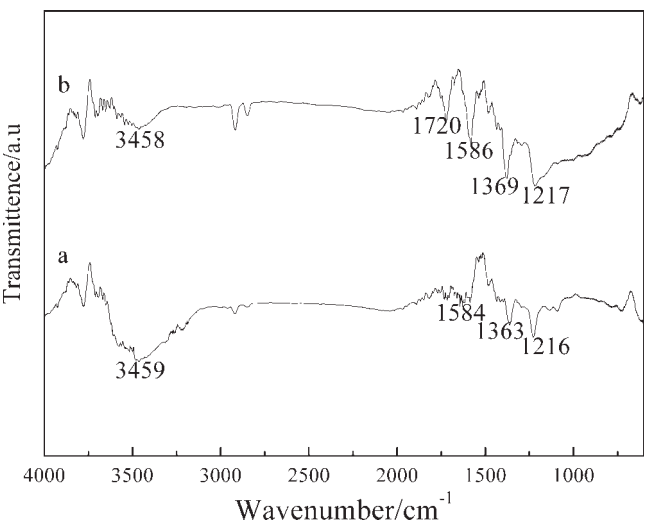

Figure 4 FTIR spectra of (a) raw MWNTs and (b) MWNTs–COOH.

TABLE I
Assignment of Peaks in the FTIR Spectrum of Carbon Nanotubes

Samples	Vibrational band (cm^{-1})	Assignment
Raw MWNTs	3459	O—H
	1586	C=C
	1363	C—H
	1216	C—O
MWNTs-COOH	3458	O—H
	1720	C=O
	1586	C=C
	1369	C—H
	1217	C—O

were finally fixed to 9 wt % in PPA. The CNTs concentration was 5 wt % with respect to the polymer.

RESULTS AND DISCUSSION

FTIR analysis of carbon nanotubes

The MWNTs–COOH were analyzed by FTIR and compared with the raw MWNTs (Fig. 4). A wide band centered at 3459 cm^{-1} was attributed to the presence of O—H groups on the surface of the raw MWNTs. The appearance was believed to result from either ambient atmospheric moisture tightly bound to the MWNTs or oxidation during purification of the raw material. The vibrational band assignments were presented in Table I.[27] After the MWNTs were treated in H_2SO_4 and HNO_3, characteristic bands due to generated polar functional groups were observed in the FTIR spectrum of the MWNTs–COOH [Fig. 4(b)]. The intensity of hydroxyl group on the surface of MWNTs–COOH was stronger than that of MWNTs. The prominent peak was present at 1720 cm^{-1}, which was assigned for C=O stretching vibrations. It indicated that carboxylic and hydroxyl groups were introduced into the surface of MWNTs. These functional groups existed at the tip and on the outer shell of the tubes, and hence easily disperse in common solvents.

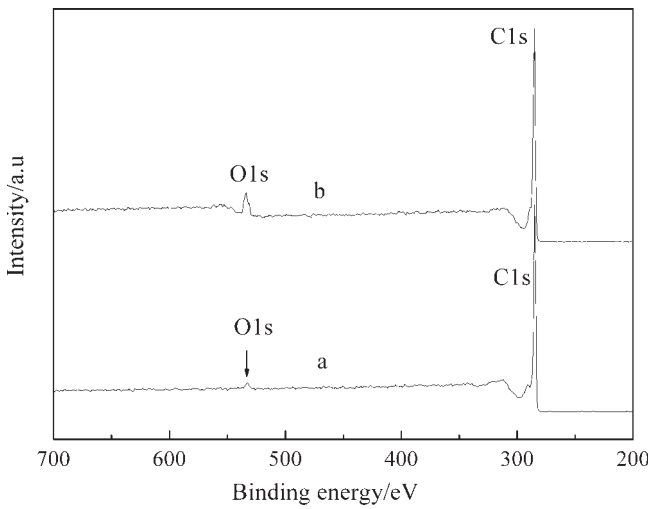

Figure 5 Typical survey XPS spectra of (a) raw MWNTs and (b) MWNTs–COOH.

TABLE II
Relative Amount of Elements on Carbon Nanotubes Surface

Samples	Relative amount of element on nanotubes surface (%) C	O	O/C
Raw MWNTs	95	5	0.05
MWNTs–COOH	87	13	0.15

XPS analysis of carbon nanotubes

XPS spectra for the raw MWNTs and the MWNTs–COOH were shown in Figure 5. The XPS data for each sample were analyzed to determine peak locations

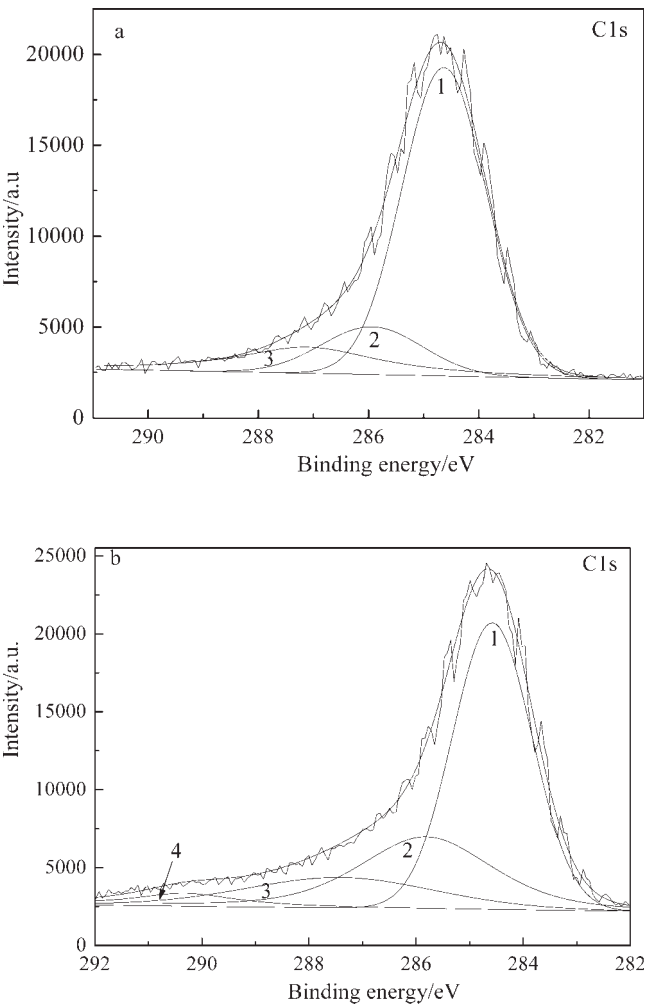

Figure 6 XPS spectra of (a) C_{1S} peak spectra by XPS analysis of raw MWNTs and (b) C_{1S} peak spectra by XPS analysis of MWNTs–COOH.

TABLE III
Relative Area (%) of C1s XPS of Carbon Nanotubes

Samples		Peak 1 C—C	Peak 2 —C—OH	Peak 3 C—O—C	Peak 4 —C=O
Raw MWNTs	Binding energy (eV)	284.6	285.9	287.1	–
	Content of functional groups (mol %)	74	14	12	–
MWNTs–COOH	Binding energy (eV)	284.6	285.8	287.4	290.3
	Content of functional groups (mol %)	58	22	13	7

and areas in relation to specific binding energies. The atomic concentration of oxygen for raw MWNTs was about 5 atomic%. However, that of MWNTs–COOH was about 13 atomic%, indicating the incorporation of polar groups having oxygen. The raw MWNTs and MWNTs–COOH of O/C area ratio determined were 0.0 5 and 0.15 respectively, by the XPS (shown in Table II).

Figure 6 showed the curve fitting of C1s for the raw MWNTs and MWNTs–COOH. The fitting of the peaks with the mixed Gaussian and Lorentzian peaks indicated a sp2 carbon- and oxygen-related peaks. Aside from the main C—C peak at 284.6eV, additional photoemission presenting at the higher binding energy bands indicated the presence of carbon atoms bonded to other functional groups for the raw MWNTs and MWNTs–COOH. The binding energy peaks at 285.9 eV and 287.1 eV for the raw MWNTs [Fig. 6(a)] were attributed to atmospheric oxidation or residual oxides resulting from the MWNTs purification process, consistent with the FTIR results discussed above. For the MWNTs–COOH sample of Figure 6(b), the additional higher binding energies at 285.8 eV, 287.4 eV, and 290.3 eV represented the C—OH, —C—O—C—, and O—C=O (carboxylic acid) contributions, respectively,[28] (shown in Table III). These results indicated that the surface of CNTs contained carbonyl groups after acid oxidated treatment.

TEM of raw MWNTs and MWNTs–COOH

The TEM images of raw MWNTs and MWNTs–COOH were shown in Figure 7. From Figure 7(a), it can be seen that the raw MWNTs aggregated into agglomerates, which led to poor dispersion. The TEM image of the MWNTs–COOH [Fig. 7(b)] showed that nanotubes had been broken into smaller pieces and were homogeneously spread. This meant that the nanotubes treated with acid were shortened, which is to say, the dispersion of nanotubes was improved in common solvents.[29]

Dispersion of carbon nanotubes in the PBO matrix

The homogeneous dispersion of CNTs in the polymer matrix was one of the most important requirements in achieving mechanical strength reinforcement because inhomogeneity could lead to structural defects in the nanocomposites material. The images of SEM and AFM showed tensile failure surface of

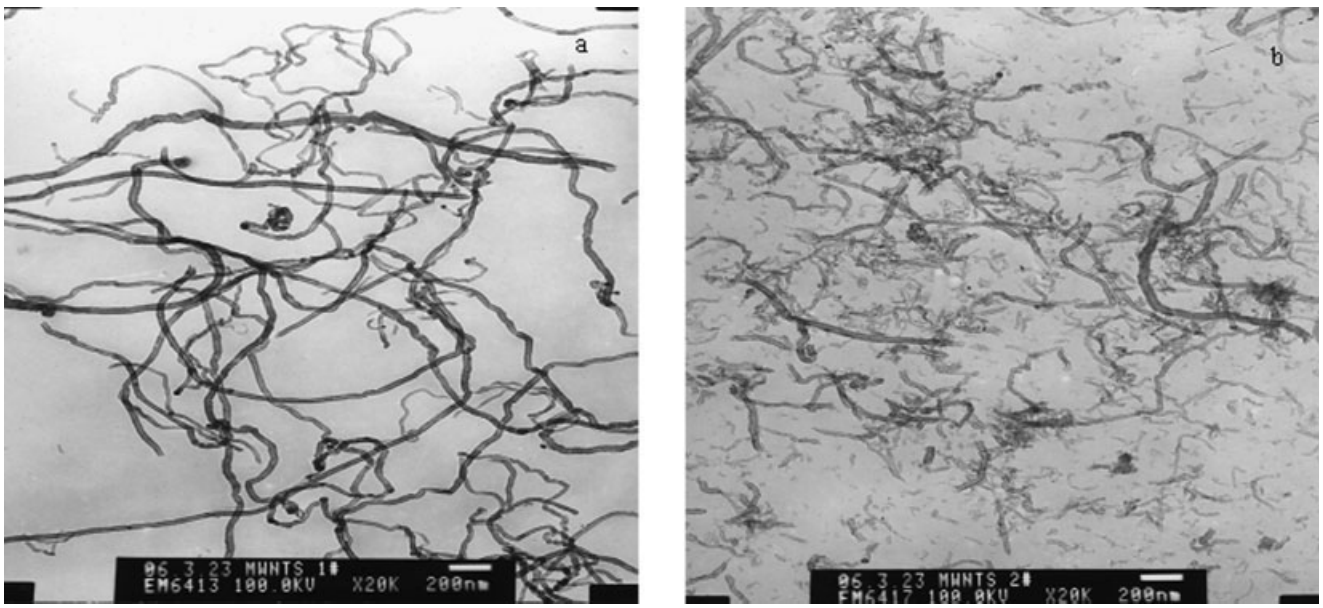

Figure 7 TEM images of (a) raw MWNTs and (b) MWNTs–COOH.

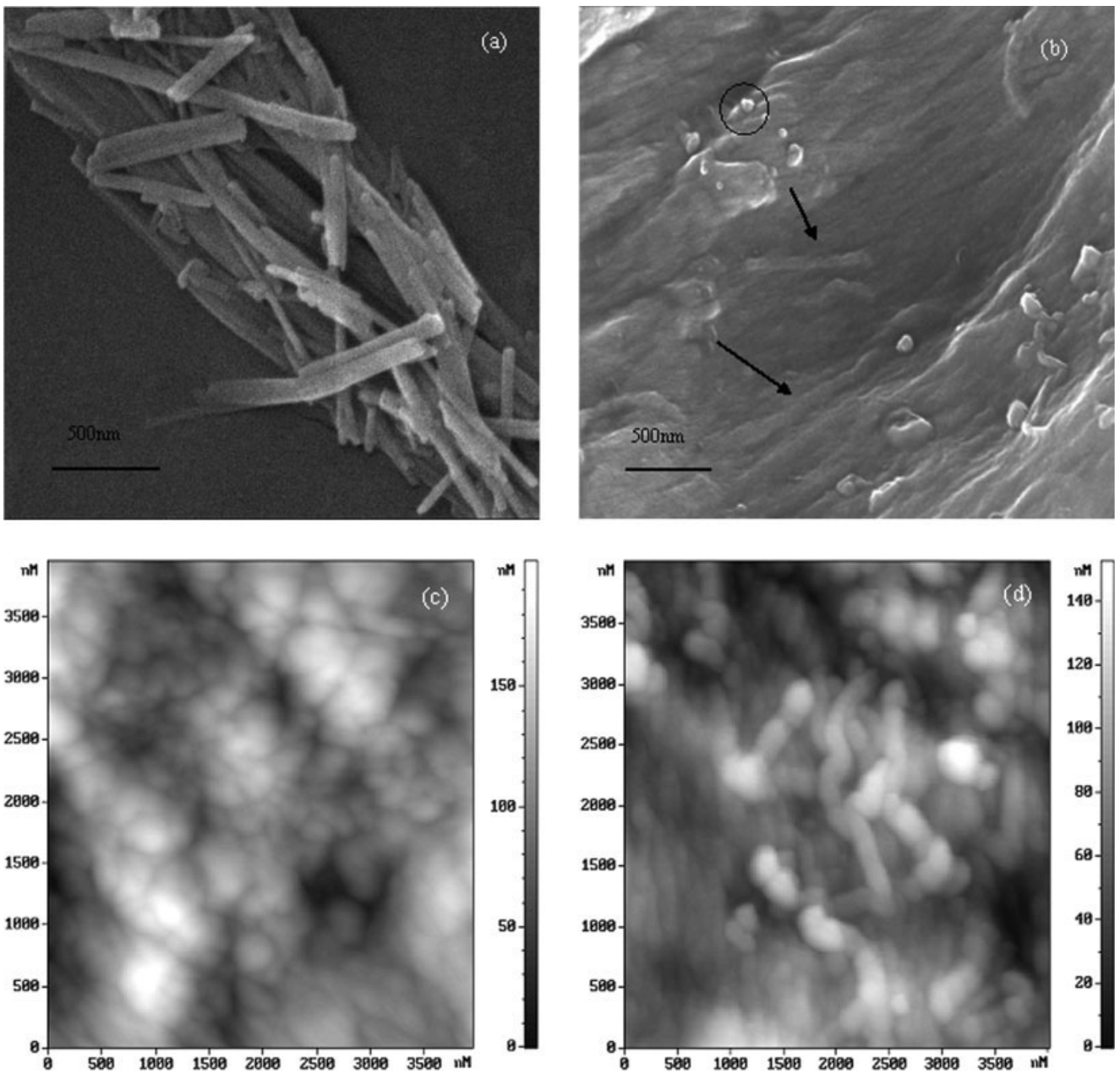

Figure 8 SEM and AFM of dispersal of CNTs in PBO matrix (a) SEM image of tensile failure surface raw MWNTs/PBO, (b) SEM image of tensile failure surface MWNTs–COOH/PBO, (c) AFM image of raw MWNTs/PBO, and (d) AFM image of MWNTs–COOH/PBO.

raw MWNTs/PBO and MWNTs–COOH/PBO nanocomposites in Figure 8. MWNTs–COOH was embedded in the PBO matrix (as seen in the ring) and direction of arrowhead showed that orient of MWNTs was consistent with that of PBO, and individual MWNTs was illustrated obviously in Figure 8(b). It was evident that the MWNTs–COOH was homogeneously distributed in the PBO matrix without aggregation. Nanotubes looked like worms in the light part of AFM image [Fig. 8(d)], and a typical size for nanotubes of MWNTs–COOH observed by AFM and SEM was approximately 100 nm. However, the aggregation of the raw MWNTs in the PBO matrix appeared in Figures 8(a and c). The images of TEM also manifested that the raw MWNTs were aggregated, but the MWNTs–COOH were evenly dispersed in the organic solvent.

Raman spectra analysis

The Raman spectra of raw MWNTs, PBO and MWNTs–COOH/PBO nanocomposites were given in Figure 9. There were two dominant optically active phonon modes in the first order Raman spectrum of the raw

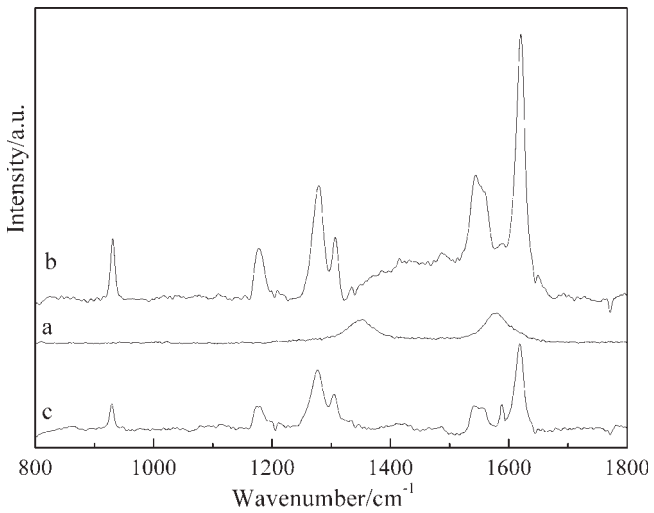

Figure 9 Raman photographs of (a) raw MWNTs, (b)PBO, and (c) MWNTs–COOH/PBO nanocompsites.

MWNTs. The line at 1581 cm^{-1} was the G line, which corresponds to the optically active in-plane E_{2g} vibrational mode, and the D line at 1334 cm^{-1} was related to the defects in CNTs.[28] The characteristic peaks of PBO,[30] that is, the peaks of 928, 1178, 1207, 1278, 1306, 1543, and 1620 cm^{-1}, were obviously observed in the spectra of both PBO polymer and MWNTs–COOH/PBO nanocomposites. However, a new peak at 1588 cm^{-1} was also observed in MWNTs–COOH/PBO nanocomposites. Because of the lack of theoretical Raman analyses upon model materials and of theoretical analyses, it had not been possible to assign them all to the molecular vibrations.

Mechanical properties analysis

Unlike carbon and inorganic fibers, polymeric fibers did not exhibit a catastrophic failure in compression. Under axial compression, polymeric fibers were fractured by kinking. From observation of sharp, high angle tilt boundaries confirmed a deformation mechanism that involved kinking of individual polymer chains. Kink band formation was a typical feature in the compression failure of oriented polymers.[31] The knot strength and tensile strength of PBO and MWNTs–COOH/PBO fibers were tested. While MWNTs were added to a loading of 5 wt %, the knot strength of PBO was increased by 30% from 1.39 cN/dtex to 1.80 cN/dtex, and the tensile strength of PBO was improved by about 33%from 1 GPa to 1.3 GPa. To reveal the possible reinforcing mechanism, the images of SEM and AFM in Figures 8(b and d) showed the dispersion of MWNTs–COOH in PBO matrix. The images clearly illustrated that the MWNTs–COOH dispersed evenly throughout the PBO matrix, which was very important for making CNT-reinforced polymer composites with excellent mechanical properties. Although the tensile strength was less than that was reported by Kumar et al.,[13] the increased percentage of tensile strength in MWNTs–COOH/PBO composites was almost equal to that in Kumar's report. If the polymerization technology is improved, the properties will be increased. The chemical reaction between PBO oligomer and MWNTs–COOH may increase the tensile strength. From Figure 8(b), it could be observed that a few MWNTs–COOH were pulled out of the matrix (as indicated by circle) and the other end still strongly

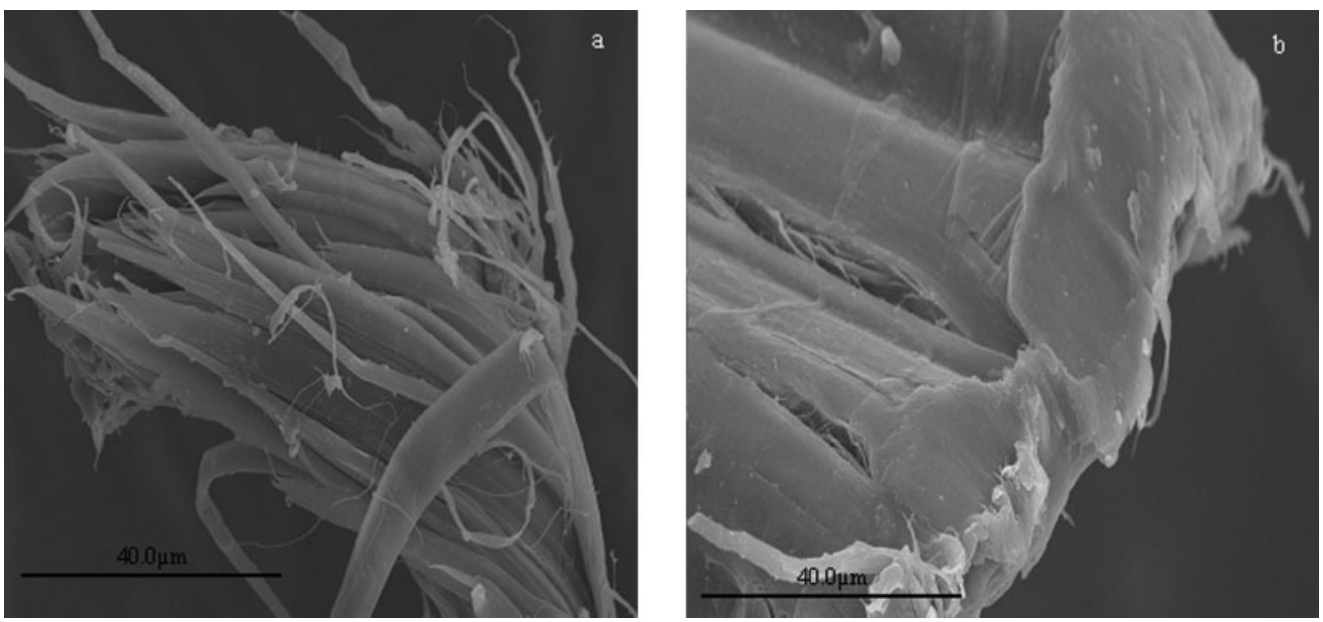

Figure 10 SEM images of (a) knot failure surface of PBO polymer and (b) knot failure surface of MWNTs–COOH/PBO composites.

embedded in the matrix. Thus, a strong interconnection existed in the matrix and the nanotubes. It was significant that the chemical reaction and strong interconnection between MWNTs–COOH and PBO could improve mechanical property.

Figure 10 showed the SEM images of the knot failure surface of PBO and MWNTs–COOH/PBO. In Figure 10(a), the fractured surface of PBO was very loose. And there were larger fibril bundles, which were slightly bent and sometimes twisted. PBO fibril bundles and fibrils had either a rounded and irregular or a ribbon-like cross section.[32] However, the fractured surface of MWNTs–COOH/PBO was tight and contained little fibrils as shown in Figure 10(b), meaning that the knot strength was higher than that of PBO. The results indicated that nanotubes had improved the intermolecular interaction of PBO.

Thermal properties analysis

MWNTs–COOH/PBO fibers and PBO fibers were characterized by differential thermal analysis (DTA) in air, and the results were shown in Figure 11. It was obvious that the melting point of MWNTs–COOH/PBO was basically consistent with that of PBO, so the molecular weight of MWNTs–COOH/PBO and that of PBO were almost identical.

Thermal degradation behavior of MWNTs–COOH/PBO in nitrogen as well as in air was compared with that of PBO in Figure 12. Both PBO and MWNTs–COOH/PBO showed an outstanding thermal stability, as there were no appreciable mass changes until 600°C under air atmosphere; but PBO nearly disappeared at almost 700°C. In nitrogen mass loss of MWNTs–COOH/PBO was less than that of PBO at the same temperature. It was evident that MWNTs–COOH/PBO nanocomposites showed better thermal stability over the investigated temperature range in either air or nitrogen.

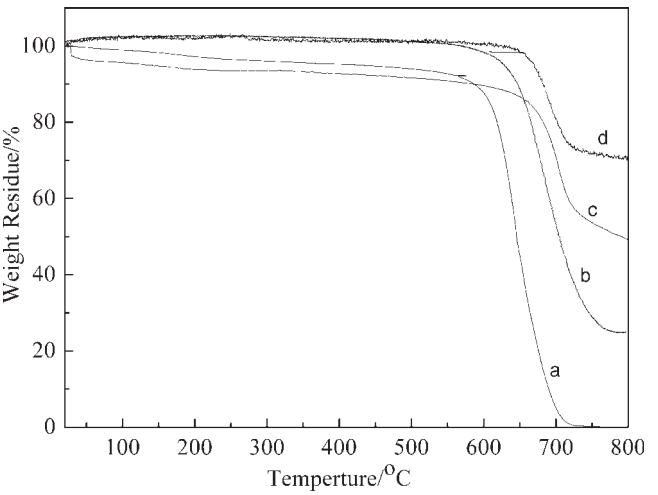

Figure 12 TG of (a) polymer, (b) MWNTs–COOH/PBO nanocomposites in air, (c) polymer, and (d) MWNTs–COOH/PBO nanocomposites in nitrogen.

Hypothesis of reaction between PBO oligomer and MWNTs–COOH

Figure 13 showed the ATR–FTIR spectra of PBO and MWNTs–PBO. In the ATR–FITIR spectrum of PBO, the wide bands centered at 3400 cm^{-1} were *N*—H and O—H stretching vibrations of amine and hydroxyl end groups, the band at 1608 cm^{-1} was assigned to C=N bonds; the bands at 1532 and 1454 cm^{-1} were assigned to skeletal vibrations of the conjugated system; the bands at 1371, 1095, and 1003 cm^{-1} were assigned to different C—H; the band at 1300 cm^{-1} were C—N band.[33] To compare bands of PBO, all characteristic PBO peaks were observed and the new

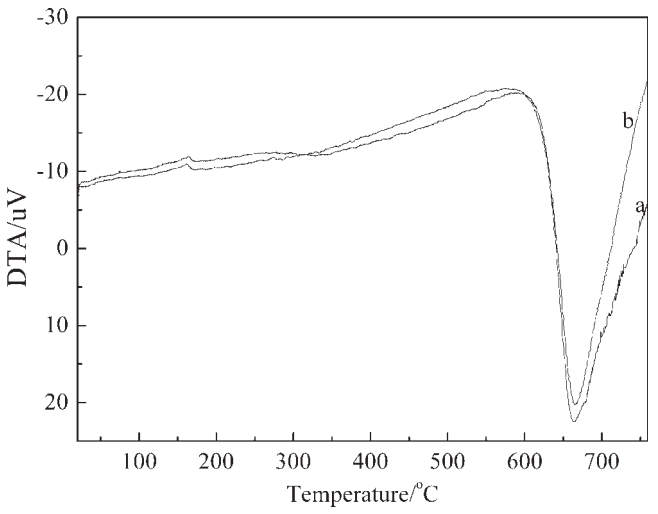

Figure 11 DTA profiles of (a) PBO and (b) MWNTs–COOH/PBO in air.

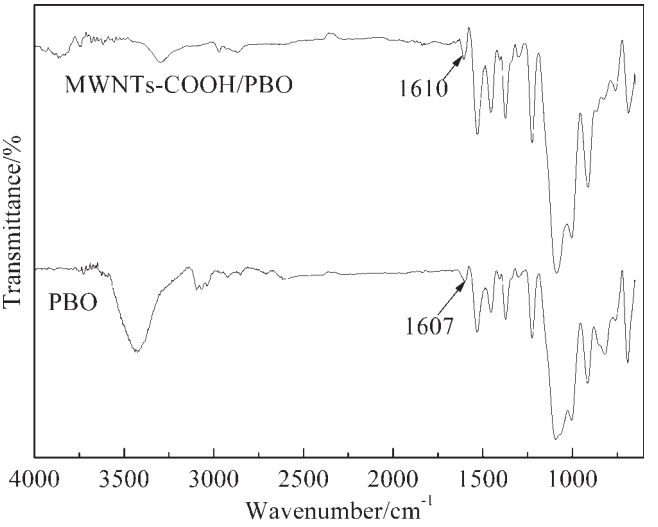

Figure 13 ATR-FTIR spectra of PBO and MWNTs–COOH/PBO.

peak of MWNTs–PBO was not found in the spectrum of MWNTs–PBO. Furthermore, one of the possible reaction routes was described in Figure 2. After treated with oxidative acid, there were some carboxyl groups introduced into the surface of MWNTs–COOH by FTIR and XPS analysis, and carboxyl groups on MWNTs–COOH reacted with the functional groups of PBO oligomer and produced the covalent bond at the interface of MWNTs and PBO.

CONCLUSIONS

The raw MWNTs were treated by strongly oxidated acid. The results of FTIR, XPS, and TEM analysis indicated that the carboxyl groups were introduced into the surface of MWNTs–COOH and the length of nanotubes was shortened. The MWNTs–COOH/PBO nanocomposites were prepared by *in situ* polymerization method. The images of SEM and AFM indicated that the MWNTs–COOH was embedded within the PBO matrix and dispersed homogeneously in the PBO matrix. The MWNTs–COOH/PBO nanocomposites had better thermal properties than PBO, and the knot strength and tensile strength were improved by 30% respectively. The nanocomposites can be used as functional materials.

References

1. Choe, E. W.; Kim, S. N. Macromolecules 1981, 4, 920.
2. So, Y. H.; Heeschen, J. P.; Bell, B. Polym Preprints 1999 40, 280.
3. Wolf, J. F.; Arnold, F. E. Macromolecules 1981, 14, 909.
4. Gregory, T. U.S. Pat. 5,194,568, 1993.
5. Jenekhe, S. A.; Johnson, P. O. Macromolecules 1990, 23, 4419.
6. Kitagawa, T.; Murase, H.; Yabuki, K. J Polym Sci Part B: Polym Phys 1998, 36, 39.
7. So, C. L.; Bennett, J. A.; Sirichaisit. J.; Young, R. J.; Liua, H. K.; Taib, N. H.; Chena, C. C. Plast Rubber Compos 2003, 32, 199.
8. Dean, D. R.; Husband, D. M.; Dotrong, M.; Wang, C. S.; Dotrong, M. H.; Click, W. E.; Evers, R. C. J Polym Sci Part A: Polym Chem 1997, 35, 3457.
9. So, Y. H.; Bell, B.; Heeschen, J. P. R.; Nyquist, A.; Murlick, C. L. J Polym Sci Part A: Polym Chem 1995, 1, 159.
10. Radler, M. J.; Landes, B. G.; Nolan, S. J.; Broomall, C. F.; Chritz, T. C.; Rudolf, P. R.; Mills, M. E.; Bubeck, R. A. J Polym Sci Part B: Polym Phys 1994, 16, 2567.
11. Khanna, D. N. Polym Preprints 1990, 5, 348.
12. Mathur, A.; Netravali, A. Text Res J 1996, 66, 201.
13. Kumar, S.; Dan, T. D.; Arnold, F. E. Macromolecules 2002, 35, 9039.
14. Iijima, S. Nature 1991, 354, 56.
15. Kwon, J. Y.; Kim, H. D. J Appl Polym Sci 2005, 96, 595.
16. Xia, H. S.; Wang, Q.; Li, K. S.; Hu, G. H. J Appl Polym Sci 2004, 1, 378.
17. Zhao, L. P.; Gao, L. Carbon 2003, 42, 423.
18. Quan, Y. D. Francois, R. J.; Edward, S. J Phys Chem B 2005, 109, 7788.
19. Lourie, O.; Wagner, H. D. Appl Phys Lett 1998, 73, 3527.
20. Amelinckx, S. D.; Bernaerts, X. B.; Zhang, T.; Van, G.; Van, L. J. Science 1995, 267, 1334.
21. Moon, J. M.; An, K. H.; Lee, Y. H.; Park, Y. S.; Bae, D. J.; Park, G. S. J Phys Chem B 2001, 105, 5677.
22. Andrews, R.; Jacques, D.; Qian, D.; Dickey, E. C. Carbon 2001, 39, 1681.
23. Strong, K. L.; Anderson, D. P.; Lafdi, K.; Kuhn, J. N. Carbon 2003, 41, 1477.
24. Liu, J.; Rinzler, A. G.; Dai, H. Science 1998, 280, 1253.
25. Schmitt, R. J.; Ross, D. S.; Wolf, J. F. U.S. Pat. 4,745,232, 1988.
26. Wofle, J. F.; Arnold, F. E. Macromolecules 1981, 4, 909.
27. Zhang, J.; Zou, H. L.; Qing, Q. Y.; Li, Y. L.; Liu, Q. W. J Phys Chem B 2003, 107, 3712.
28. Ramanathan, T.; Fisher, F. T.; Ruoff, R. S.; Brinson, L. C. Chem Mater 2005, 17, 1290.
29. Wang, Y.; Wu, J.; Wei, F. Carbon 2003, 41, 2939.
30. Kitagawa, T.; Yabuki, K.; Young, R. J. Polymer 2001, 42, 2101.
31. Martin, D. C.; Thomas, E. L. J Mater Sci 1991, 26, 5171.
32. Krause, S. J.; Haddock, T. B.; Vezie, D. L. Polymer 1988, 29, 1354.
33. Shen, D. Y.; Hsu, S. L. Polymer 1982, 23, 969.